energies

MDPI

Article

Methods of Determining Pressure Drop in Internal Channels of a Hydraulic Motor

Pawel Sliwinski * and Piotr Patrosz

Faculty of Mechanical Engineering and Ship Technology, Gdansk University of Technology, 80-233 Gdansk, Poland; piotr.patrosz@pg.edu.plnd
* Correspondence: pawel.sliwinski@pg.edu.pl

Abstract: In this paper, new methods for determining the pressure drop in internal channels of a hydraulic motor are proposed and described. Mathematical models of pressure losses in internal channels have also been described. Experimental tests of the satellite motor were carried out according to one of the proposed methods. The tests were carried out for two liquids, i.e., water and mineral oil. Experimental studies have shown that at a high flow rate in the motor supplied with water the pressure losses are a dozen or so percent greater than in the motor supplied with oil. However, at low flow rates is the inverse, that is, the pressure losses in the motor supplied with water are about ten percent lower than in the motor supplied with oil. The CFD calculation of the pressure drop in the internal channel of the motor was also conducted. It was assumed that holes in the commutation unit plate are placed face to face and that the liquid did not cause changes in the working chambers' volume. In this way, it has been proven that those simplified assumptions can have up to a 50% difference in relation to the experimental tests.

Keywords: k pressure losses; satellite motor; water; oil; CFD calculation; internal channels in motor; pressure efficiency

Citation: Sliwinski, P.; Patrosz, P. Methods of Determining Pressure Drop in Internal Channels of a Hydraulic Motor. *Energies* **2021**, *14*, 5669. https://doi.org/10.3390/en14185669

Academic Editor: Ryszard Dindorf

Received: 4 August 2021
Accepted: 3 September 2021
Published: 9 September 2021

1. Introduction

The task of a hydraulic motor is to convert hydraulic energy into mechanical energy. Liquid is an energy carrier in the hydraulic system. Currently, mineral oil is the most commonly used liquid in hydraulic systems [1]. However, in some industrial sectors, a liquid that is non-flammable (mining, steel mills, etc.) or non-toxic for the environment and human health (food industry) is required [2].

Water is a liquid which is non-flammable, non-toxic and certainly suitable for energy transfer in hydraulic systems. Furthermore, water is generally available as a working liquid. There is a growing trend throughout the world towards researching and developing components and hydraulic systems that are supplied with water [1–4]. The development of water hydraulics is important for various industrial sectors, e.g., for the food industry, the mining industry and marine technology [5]. In comparison to mineral oil, water has a very low viscosity and low lubricating properties [6]. These features adversely influence the efficiency of energy conversion in hydraulic systems [7]. Despite this, attempts are being made to develop innovative components and hydraulic systems supplied with water [2].

Each hydraulic element (pump, motor and valves) is recommended to a specific type of working liquid. For example, a hydraulic motor recommended to oil circuits should not be used in water systems. In other cases, this motor has very little durability and a low efficiency [7]. Both the pump and the hydraulic motor are components of the hydraulic system that have large energy losses, including volumetric, mechanical and pressure losses [1,7–16].

The main sources of volumetric losses in hydraulic motors are the leakage in the clearances of the working mechanism, the leakage in the clearances of the commutation unit and the compressibility of liquid in the death chamber of the working mechanism [7–11,17–25]. However, the main sources of mechanical losses are friction between moving parts of the working mechanism and friction in bearings and seals [22,25]. In the case of pressure losses in hydraulic motors, this pressure loss results from internal channels in the motor. The internal channels are defined as channels inside the motor body. Their task is to supply liquid from the motor inflow port to the working chambers (inflow channels) and remove the liquid from the working chambers to the outflow port (outflow channels). The pressure drop in internal channels of the motor mainly depends on the geometric dimensions of those channels, the liquid parameters (viscosity and density) and the flow rate of the liquid. The pressure drop in internal channels of the motor has a significant impact on the energy conversion efficiency in the motor and on the parameters of hydraulic systems [8,11,17,22,26–28].

The results of this research proved that all of the above-mentioned types of losses were influenced by the type of liquid. In general, a motor supplied with a low viscosity liquid generates larger energy losses than a motor supplied with oil [20–23]. Thus far, there are no research results comparing the influence of water and mineral oil on the pressure losses in hydraulic motors. There is also no specific information about the designs of motors that can be supplied with both water and mineral oil. There is a rich literature on flows in orifices and other simple openings; however, there are not any prominent studies in the literature that compare the influence of the type of liquid on the flow characteristics in these internal channels.

Therefore, from the scientific and cognitive point of view, researching and describing the influence of water and mineral oil on pressure losses in a hydraulic motor is appropriate and justified. The issue of the influence of the type of liquid on the pressure losses in the hydraulic motor is a new issue, represents an important scientific problem and is the subject of this article. Consequently, the following objectives have been defined for this article:

(a) Describe a mathematical model of the pressure losses;
(b) Results of experimental tests of pressure in working chambers and pressure losses in motor supplied with mineral oil and water and their comparison;
(c) Results of CFD calculations of pressure losses in motor supplied with mineral oil and water and their comparison;
(d) Compare the results of experimental research with CFD calculations.

The experimental research on the influence of the type of liquid on pressure losses was carried out using a prototype of a hydraulic satellite motor presented in Section 6. The satellite motor was chosen to test because the authors of this publication are the co-creators of this motor and have conducted extensive research on the development of this motor. This motor is already produced but not yet widely known in the world.

2. Pressure Drop in the Internal Channels of the Hydraulic Motor

In the hydraulic motor the pressure drop Δp_{ich} in internal channels increases the value of the pressure drop Δp. The pressure drop Δp is measured in motor ports (Figure 1), according to the formula [29]:

$$\Delta p = \Delta p_i + \Delta p_{ich} \quad (1)$$

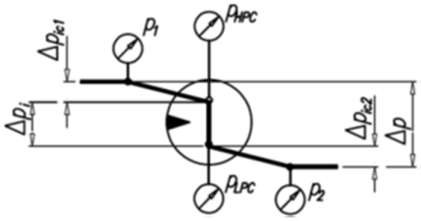

Figure 1. Pressure drop in hydraulic motor [23]: Δp_{ic1}—pressure drop in inflow internal channel, Δp_{ic2}—pressure drop in outflow internal channel, p_{HPC}—pressure in high-pressure working chamber, p_{LPC}—pressure in low-pressure working chamber, p_1—pressure in inflow motor port, p_2—pressure in outflow motor port.

Pressure drop Δp_{ich} in internal channels is the following sum [29]:

$$\Delta p_{ich} = \Delta p_{ic1} + \Delta p_{ic2} \quad (2)$$

where:

- Δp_{ic1}—the pressure drop in inflow internal channel;
- Δp_{ic2}—the pressure drop in outflow internal channel.

In a hydraulic motor with variable shaft rotation directions, if the inflow and outflow internal channels in a hydraulic motor have the same shape and dimensions then is only necessary to measure Δp_{ic1} and the Δp_{ich} is calculated according to the formula:

$$\Delta p_{ich} = 2 \cdot \Delta p_{ic1} \quad (3)$$

3. Known Method for Measuring the Pressure Drop in Internal Channels—Method 1

The measurement of pressure drop in internal channels of hydraulic motor during his normal work is problematic. The main problem is the pressure measurement in working chambers; it is technologically difficult to implement or sometimes impossible. Therefore, it is easier to determine the pressure drop in internal channels of a hydraulic motor if this motor works as a pump.

In known method the test stand is equipped with a drive motor *DM* with constant speed and does not include an electronic measurement data recording system (Figure 2). Changes in the setting of the throttle valve *TV* in a low-pressure line are made and the pressure p_1 in the low-pressure port of motor (suction port—motor works as a pump) is measured. The flow rate Q is measured at the moment of cavitation in the motor. Then, during cavitation, a certain value of pressure p_{LPC} in the low-pressure working chambers of the motor should be assumed. Usually, for simplicity, a vacuum of 1 bar is assumed (p_{LPC} = –1 bar) [9,15,17].

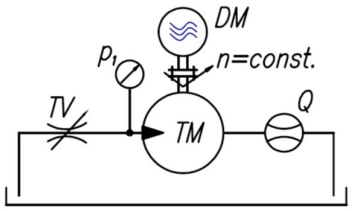

Figure 2. Scheme of the hydraulic circuit of the test stand for the measurement of the pressure drop in the internal channel of the hydraulic motor [23]: *TM*—tested motor; *DM*—drive motor; *TV*—throttle valve; Q—flow meter; p_1—manometer.

The experiment execution time is relatively short. The appearance of cavitation in the engine's working chambers does not cause damage in such a short time.

4. Proposed Methods for Measuring the Pressure Drop in Internal Channels

The disadvantages of method 1 are:

- The difficulty to catch the beginning of cavitation;
- The constant speed of motor *DM* (Figure 2) prevents the full characteristics of the pressure drop in the internal channel from being obtained;
- Unknown values of pressure in working chambers. Thus, the value of -1 bar in low-pressure working chamber was assumed.

Therefore, new methods that avoid this inconvenience are proposed below.

4.1. Method 2

Method 2 is the experimental method. In this method, similar to method 1, the hydraulic motor 1 works as a pump and is driven by an electric motor *DM* (Figure 3). The speed n of electric motor *DM* and machine 1 is set via a frequency converter. The displacement machine 1 is supplied by a pump 3 through throttle valve *TV*. At a particular setting of the valve 4, the speed n is increased from its minimum value. A recording data system collects the values of the speed n, delivery Q and pressure p_1. In this way, the characteristics of $Q = f(n)$ and $p_1 = f(n)$ are created (Figure 4). After some characteristic point 1 (Figure 4), the delivery Q does not change despite the increase in the rotational speed n. Point 1 is necessary to register the flow rate Q_1 and the pressure $p_{1\text{-}1}$. In the next step, the rotational speed n is decreased to its minimum, the setting of valve *TV* is changed, and, at the end, the speed n is increased again and the values of n, Q and p_1 are registered. In this way, the point 2 (parameters Q_2 and $p_{1\text{-}2}$) are obtained. In order to obtain the full characteristics of the pressure drop in the internal channel of the motor, this procedure should be carried out several times with different settings of valve *TV*.

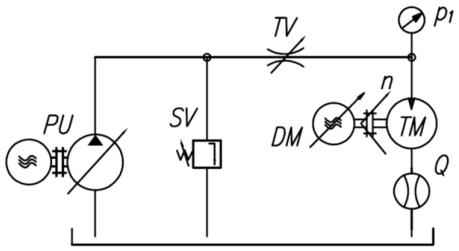

Figure 3. Scheme of hydraulic circuit of the test stand for the measurement of the pressure drop in the internal channel of the hydraulic motor according to method 2: *TM*—tested motor, *DM*—drive motor, *PU*—pump unit, *TV*—throttle valve, *SV*—safety valve, *Q*—flow meter, p_1—manometer (pressure in inflow port of motor), n—rotational speed.

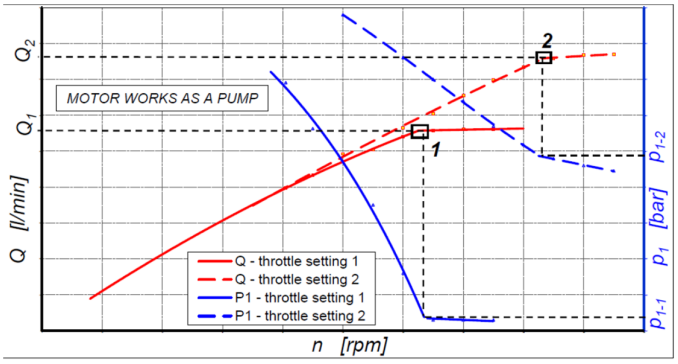

Figure 4. Delivery Q of motor 1 working as a pump and the pressure p_1 in the suction port of motor 1 for two different settings of throttle valve *TV*—according to the scheme in Figure 3 [23].

For points 1,2,...,n (Figure 4) in the suction working chambers of tested motor TM, there exists pressure p_{LPC} close to the vacuum. Therefore, the pressure drop Δp_{ic1} in the internal channel (from the inflow (suction) port of the motor, which is p_1, to the suction working chambers) is:

$$\Delta p_{ic1} = p_1 - p_{LPC} \quad (4)$$

For a hydraulic motor with the same internal channels on the inflow and the outflow side, the total pressure drop Δp_{ich} is calculated according to formula (3). Theoretical characteristics $\Delta p_{ich} = f(Q)$ are shown in Figure 5.

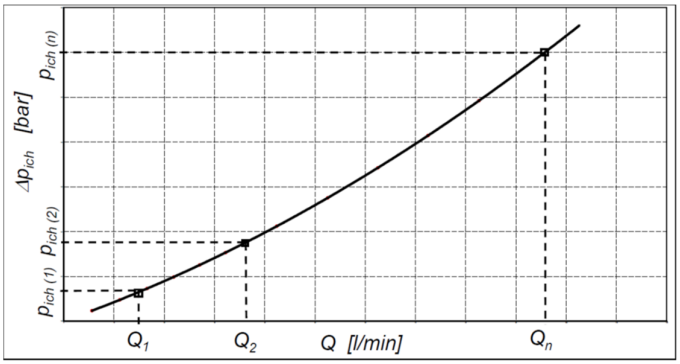

Figure 5. Theoretical characteristics of $\Delta p_{ich} = f(Q)$ [23].

4.2. Method 3

Method 3 is the experimental method. In this method, similar to methods 1 and 2, the hydraulic motor *TM* works as a pump and is driven by an electric motor *DM*. The speed n of the electric motor *DM* and tested motor *TM* is set via a frequency converter (Figure 6). In this method, a measurement data acquisition system at the same time records:

(a) The pressure p_1 and p_2 in motor ports;
(b) The pressure p_{LPC} and p_{HPC} in motor working chambers;
(c) The delivery Q;
(d) The rotational speed n of the motor shaft.

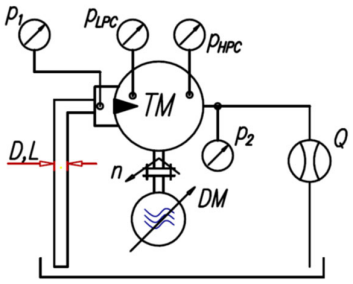

Figure 6. Hydraulic circuit of the test stand for the measurement of the pressure drop in the internal channel of the hydraulic motor according to method 3: D—diameter of suction tube, L—length of suction tube, *TM*—tested motor, *DM*—electric motor (controlled by frequency converter), Q—flow meter, n—rotational speed, p_{HPC}—pressure in high-pressure working chamber, p_{HPC}—pressure in low-pressure working chamber, p_1—pressure in inflow motor port, p_2—pressure in outflow motor port.

If cavitation occurs in the low-pressure working chamber, then the increase in rotational speed n of the tested motor does not increase the flow rate Q in this motor. This is because the pressure drop between the tank and low-pressure chamber is constant (in tank is zero and in the low-pressure chamber during full cavitation the pressure is also

constant). If the pressure drop is constant, then the flow rate Q also must to be constant. Therefore, for Q = const. is incomplete filling of the working chamber.

In all described methods the flow meter was located in the outflow hose of the motor. This flow meter creates considerable resistance to flow (the pressure p_2 in the drain connection is greater than zero). So, a throttle valve to increase pressure p_2 was not needed and the cavitation in the low-pressure working chamber has no influence on the measurement of flow rate Q.

At the stage of theoretical considerations, it can be assumed that the pressure drop in the internal channels of the motor depends on the type of overlap in the commutation unit of the working mechanism. Therefore, in a motor with the negative overlap in the commutation unit (especially on the high-pressure side) there is no additional pressure increase caused by liquid compression in the closed working chamber. Then, the pressure drop is calculated according to Formula (1) considering (Figure 7.):

$$\Delta p_{ic1} = p_1 - p_{LPC} \quad (5)$$

$$\Delta p_{ic2} = p_{HPC} - p_2 \quad (6)$$

However, in a motor with the positive overlap or zero overlap in the closed working chamber additional increase in pressure is created. Furthermore, the higher the rotational speed of the shaft, the higher the p_{HPC} in the working chamber. Therefore, the pressure drop is calculated as (Figure 9):

$$\Delta p_{ich} = \Delta p_{ic1} + \Delta p_{ic2-L} \quad (7)$$

where:

$$\Delta p_{ic2-L} = p_{2-L} - p_{HPC-L} \quad (8)$$

- $p_{2\text{-}L}$—the pressure in port B measured for the opposite direction of the shaft rotation (rotation to the left);
- $p_{HPC\text{-}L}$—the pressure in the suction chamber measured for the opposite direction of the shaft rotation (rotation to the left).

In order to be abundantly clear, the suction working chamber with pressure p_{LPC} becomes a high-pressure working chamber with pressure $p_{LPC\text{-}L}$ after changing the direction of rotation. However, a high-pressure working chamber with pressure p_{HPC} becomes a low-pressure working chamber with pressure $p_{HPC\text{-}L}$ after changing the direction of rotation.

Theoretical characteristics of the pressure drop in internal channels of a hydraulic motor are represented exactly as Figure 5 shows.

An increase of pressure Δp_{HPC} in a high-pressure working chamber caused by compression of liquid is:

$$\Delta p_{HPC} = \Delta p_{ic2} - \Delta p_{ic2-L} \quad (9)$$

Thus, the change of pressure in the hydraulic motor should progress as in Figure 7. The increase of pressure Δp_{HPC} has a direct influence on the mechanical losses in the working mechanism. Therefore, the Δp_{HPC} is not the component of the pressure losses in the internal channels of the motor [23,29].

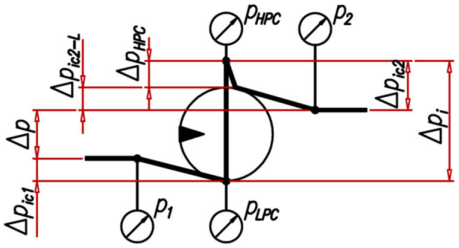

Figure 7. The progress of pressure in a hydraulic motor (working as a pump) including the increase of pressure Δp_{HPC} in a high-pressure working chamber.

In a hydraulic motor with a variable direction of shaft rotation the internal channels on the supply side and on the outflow side have the same dimensions. Then, the total pressure drop Δp_{ich} can be calculated according to Formula (3).

4.3. Method 4

Method 4 is also the experimental method. Is this method, the pressure drop is measured in a loaded hydraulic motor equipped with pressure sensors like in Figure 1. In this method, the test stand must be able to set the motor speed. The measurement data recording system is not required.

Due to the fact that method 4 is analogous to methods 2 and 3, it will not be described.

4.4. Practical Aspects of Applying the Methods 2 and 3

From the practical point of view the biggest disadvantages of method 3 is necessity of measurement of the pressure in the working chamber of the tested machine. Therefore, this method rather will not be used in some types of positive displacement machines, like in an axial piston pump or motor. However, in other displacement machines (like in satellite displacement machines) the possibility of measurement of the pressure in the working chamber is a very important advantage because it is easy to obtain the characteristics of pressure drop Δp_{ic1} and Δp_{ic2} in internal channels. The measurement of pressure p_1 and p_{HPC} (and similarly p_2 and p_{LPC}) gives higher accuracy of the characteristic $\Delta p_{ic1} = f(Q)$ (or $\Delta p_{ic2} = f(Q)$) in all ranges of Q. This is not possible in method 2, where the pressure p_{LPC} has to be assumed.

Method 2 requires a more advanced test stand (additional pump and throttle valve) and larger number of measurement series than method 3. Furthermore, method 3 makes it possible to designate an increase of pressure Δp_{HPC} in a high-pressure working chamber caused by compression of liquid.

5. Mathematical Models of the Pressure Drop in the Internal Channels of the Hydraulic Motor

The pressure drop Δp_{ich} in the internal channels of the hydraulic motor is energetic losses and is commonly called "pressure losses". The geometry of the internal channels (shape and dimensions) has influence on the value of the pressure drop. Any changes in the channel geometry has a large influence on the direction of the liquid flow and on the average liquid flow speed c. In this way, the pressure drop Δp_{ich} is treated as a local pressure loss. The local pressure loss is described by the well-known formula:

$$\Delta p_{ich} = \xi \cdot \rho \cdot \frac{c^2}{2} \quad (10)$$

where:

- ξ—the coefficient of pressure loss;
- ρ—the density of liquid.

In the case of hydraulic machines, the coefficient of pressure loss is expressed by the formula [17]:

$$\xi = \frac{C_1}{Re} + C_2 \tag{11}$$

where C_1 and C_2 are constants.

In a hydraulic motor, the internal channels are short and have irregular geometry, so it is not possible to calculate Reynolds number Re and the average speed c in this way. However, it is known that $Re = f(c)$ and $c = f(Q)$. Therefore, the pressure losses in internal channels of the motor can described by:

$$\Delta p_{ich} = \underbrace{C_t \cdot \rho \cdot Q^2}_{turbulent\ flow\ component} + \underbrace{C_l \cdot \nu \cdot \rho \cdot Q}_{laminar\ flow\ component} \tag{12}$$

where:

- C_t—the constant of turbulent flow component;
- C_l—the constant of laminar flow component;
- ν—the kinematic viscosity.

The advantages of the above model are [29]:

(a) The geometry of the motor's internal channels is omitted;
(b) The pressure losses are expressed as a function of density and viscosity of the liquid and the liquid flow rate (these are the parameters having a direct impact on the pressure losses);
(c) The values of constants C_t and C_l can be calculated based on the equation of the trend line of the characteristic shown in Figure 5.

In the literature, the pressure losses Δp_{ich} are also described by the following formula [17,27]:

$$\Delta p_{ich} = C_{ich} \cdot \rho \cdot \omega^2 \cdot \sqrt[3]{\left(\frac{V_t}{2 \cdot \pi}\right)^2} \tag{13}$$

where:

- ω—the angular speed of the motor shaft;
- V_t—the theoretical displacement;
- C_{ich}—the coefficient.

The disadvantages of the above model are as follows:

(a) The angular speed ω has an indirect influence on the pressure drop Δp_{ich} in the internal channels because angular speed is a function of theoretical absorbency Q_t of the motor and a function of volumetric losses Q_{vl} in the motor. Thus, only the absorbency Q (flow rate consumed by the motor) has influence on Δp_{ich}. The absorbency Q is defined as:

$$Q = Q_t + Q_{vl} \tag{14}$$

(b) Theoretical displacement V_t has influence only on the theoretical absorbency Q_t;
(c) Does not take into account the influence of liquid viscosity on the pressure drop. The flow in internal channels is assumed as turbulent flow only.

Z. Paszota describes the pressure losses in the internal channels of the motor in the following way [11]:

$$\Delta p_{ich} = k_8 \cdot p_n \cdot \left(\frac{Q}{Q_{pt}}\right)^{a_{Qp}} \cdot \left(\frac{\nu}{\nu_n}\right)^{a_{vp}} \tag{15}$$

where:

- k_8—the coefficient determining the pressure loss in the internal channels and in the commutation unit of the motor;
- a_{Qp}—the exponent of the influence of the liquid flow rate in the internal channels on pressure losses;
- a_{vp}—the exponent of the influence of liquid viscosity on pressure losses;
- p_n—the nominal pressure of the pump;
- Q_{Pt}—the theoretical delivery of the pump;
- ν_n—the reference viscosity of the liquid.

The inconvenience of the above model is the dependence of the pressure drop Δp_{ich} on the parameters of the pump supplying the motor. Furthermore, it is necessary to assume the reference viscosity ν_n of the liquid. Therefore, the exponents a_{Qp} and a_{vp} and the coefficient k_8 depend on the parameters of the pump and on the reference viscosity of the liquid.

6. Tested Motor

The experimental research was carried out with the use of the prototype of a satellite motor (Figures 8 and 9). The working mechanism of this motor is a satellite mechanism (Figure 10). On both sides of this mechanism are distribution plates (Figure 9 and Figure 11). The principle of operation of this mechanism and principle of operation of a satellite motor are widely described in many publications, such as in [8,20–23,29–32].

Figure 8. General view of hydraulic satellite motor (SM type) [30].

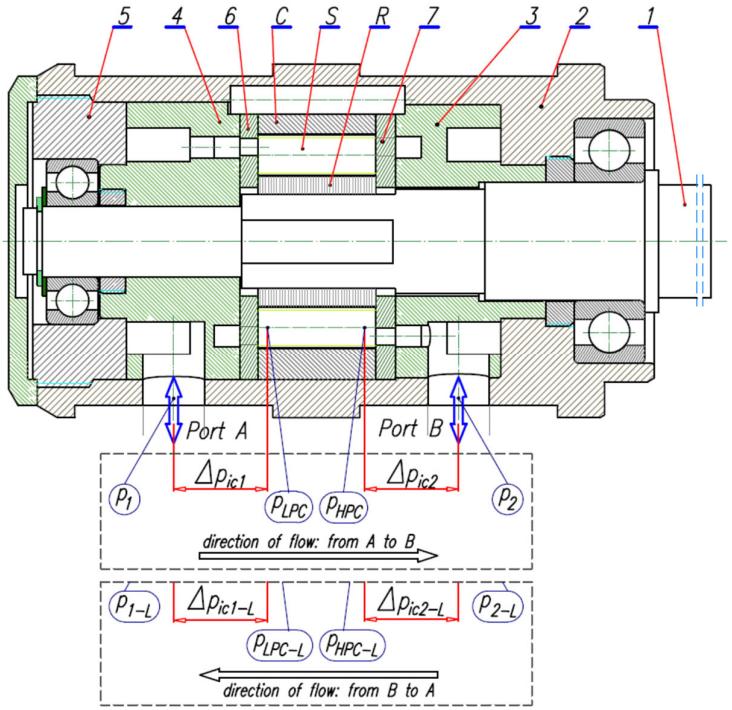

Figure 9. Construction of satellite motor and pressure drops in internal channels: *C*—curvature (stator), *S*—satellite, *R*—rotor, 1—shaft, 2—casing, 3 and 4—inflow and outflow manifolds, 5—rear plate, 6 and 7—distribution plates.

The toothed unit, shown in Figure 10, is the satellite working mechanism of the motor. It consists of a toothed rotor R (4 humps), toothed stator C (6 humps) and ten wheels S (satellite).

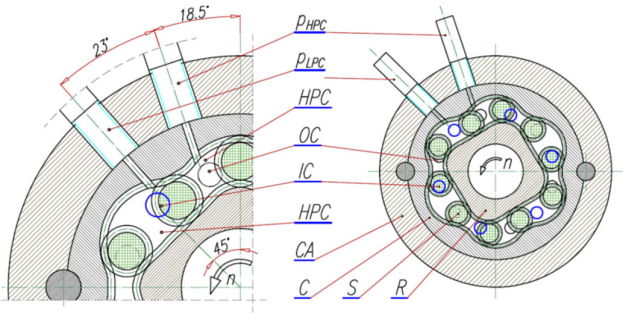

Figure 10. The cross section of the motor through the working mechanism and the location of pressure sensors p_{LPC} and p_{HPC} [23,32]: *C*—curvature (stator), *R*—rotor, *S*—satellite, *CA*—casing, *LPC*—low-pressure working chamber, *HPC*—high-pressure working chamber, *IC*—inflow hole, *OC*—outflow hole.

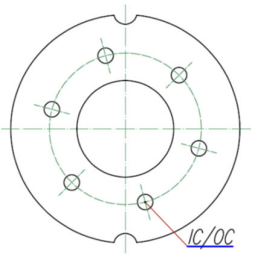

Figure 11. Distribution plate: *IC*/*OC*—inflow/outflow hole [23].

The principle of operation of satellite motor was widely described in [20-23].

The satellite motor used for the test had the following geometrical parameters [30,31]:

- The theoretical displacement q_t = 32.94 cm³/rev.;
- The teeth module m = 0.75 mm;
- The height of working mechanism H = 25 mm.

7. Results of the Research on the Pressure Drop in the Internal Channels of the Motor

In Section 4 it was written that method 3 makes it possible, besides the pressure drop Δp_{ich}, to designate an increase of pressure Δp_{HPC} caused by compression of liquid in a high-pressure working chamber. Therefore, the research on the pressure drop in the internal channels of the satellite motor was carried out according to method 3.

During the experiment the following parameters were recorded:

(a) p_1 and p_2—pressures in motor ports;
(b) p_{LPC} and p_{HPC}—pressures in motor working chambers;
(c) Q—liquid stream feeding the motor;
(d) n—the rotational speed of the motor shaft.

All pressures were measured by a strain gauge pressure transducer with range −1÷3 bar and class 0.3. The flow rate Q was measured by mass flow meter with range 33 lpm and class 0.1 and the rotational speed n was measured using the inductive sensor.

During the test the temperature of the liquid in the test stand was kept constant. The temperature of liquid in the inflow port of motor was controlled. In this way viscosity of the liquid was controlled. This temperature was not registered.

7.1. Working Liquids

Laboratory research on the pressure drop in the internal channels of the satellite motor was carried out using the following liquids:

(a) Tap water (ν = 0.9 cSt and ρ = 999.8 kg/m³);
(b) Mineral oil (ν = 40 cSt and ρ = 862.0 kg/m³).

7.2. Experimental Data—Motor Supplied with Water

In the tested motor (Figures 8 and 9), the internal channels on the supply side have the same dimensions as the internal channels on the outflow side. Therefore, it is enough to measure only Δp_{ic1}. Then, the total pressure drop Δp_{ich} in the internal channels of the motor can be calculated according to Formula (3).

The recorded results of pressure p_1, p_2, p_{HPC}, p_{LPC} and flow rate Q in the motor as a function of the shaft speed n are shown in Figure 12. In addition, characteristics Δp_{ic1} and Δp_{ic2}, whose values were calculated according to Formulas (5) and (6), are shown in Figure 13. Cavitation occurs (the flow rate Q = const.) at rotational speeds above 630 rpm. In Figure 14, characteristics Δp_{ic1} and Δp_{ic2} are shown at speeds up to 630 rpm—cavitation does not occur at these speeds.

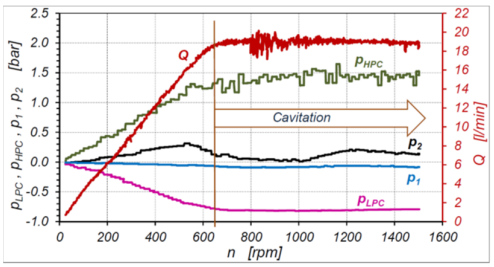

Figure 12. Characteristics of $p_1 = f(n)$, $p_2 = f(n)$, $p_{HPC} = f(n)$, $p_{LPC} = f(n)$ and $Q = f(n)$ over the entire range of the motor shaft speed n—motor supplied with water [2323].

The results of the research on the motor supplied with water show (Figure 12) that in a low-pressure working chamber LPC (Figure 10), during cavitation, the minimum value of the pressure p_{LPC} was –0.85 bar.

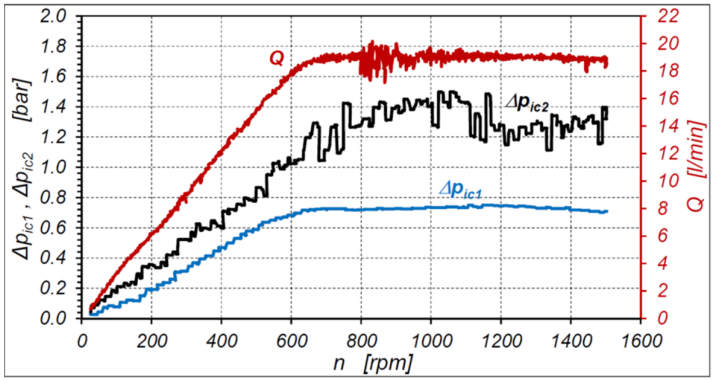

Figure 13. Characteristics of pressure drop $\Delta p_{ic1} = f(n)$ and $\Delta p_{ic2} = f(n)$ in the internal channels of the motor over the entire range of the motor shaft speed n—motor supplied with water [23].

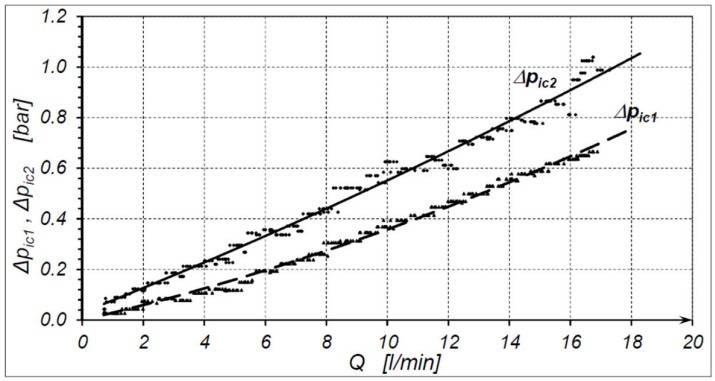

Figure 14. Characteristics of the pressure drop $\Delta p_{ic1} = f(Q)$ and $\Delta p_{ic2} = f(Q)$ in internal channels of the motor supplied with water (no cavitation) [23].

7.3. Experimental Data—Motor Supplied with Oil

The recorded results of pressure p_1, p_2, p_{HPC}, p_{LPC} and flow rate Q of oil in the motor as a function of the shaft speed n are shown in Figure 15. Characteristics Δp_{ic1} and Δp_{ic2}, whose values were calculated according to Formulas (5) and (6) are shown in Figure 16. At rotational speeds above 550 rpm, cavitation occurs (the flow rate Q = const.). In Figure 17, characteristics Δp_{ic1} and Δp_{ic2} are shown at speeds up to 580 rpm—cavitation does not occur at these speeds.

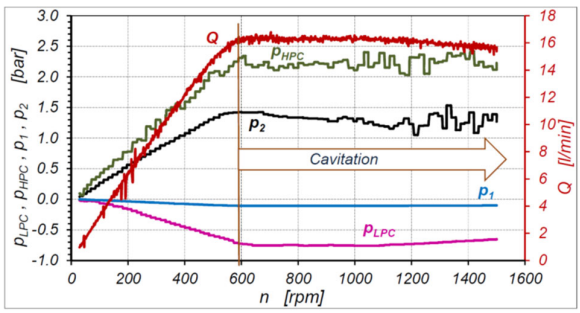

Figure 15. Characteristics of $p_1 = f(n)$, $p_2 = f(n)$, $p_{HPC} = f(n)$, $p_{LPC} = f(n)$ and $Q = f(n)$ over the entire range of the motor shaft speed n—motor supplied with oil [23].

The results of the research on the motor supplied with oil shows (Figure 15) that in a low low-pressure working chamber *LPC* (Figure 10), during cavitation, the minimum value of the pressure p_{LPC} was –0.75 bar.

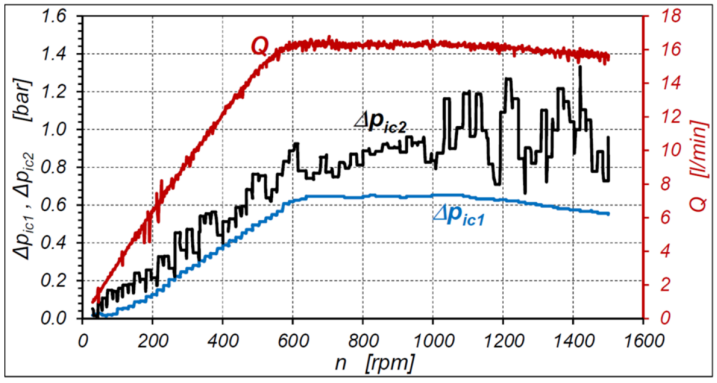

Figure 16. Characteristics of pressure drop $\Delta p_{ic1} = f(n)$ and $\Delta p_{ic2} = f(n)$ in the internal channels of the motor over the entire range of the motor shaft speed, n—motor supplied with oil [23].

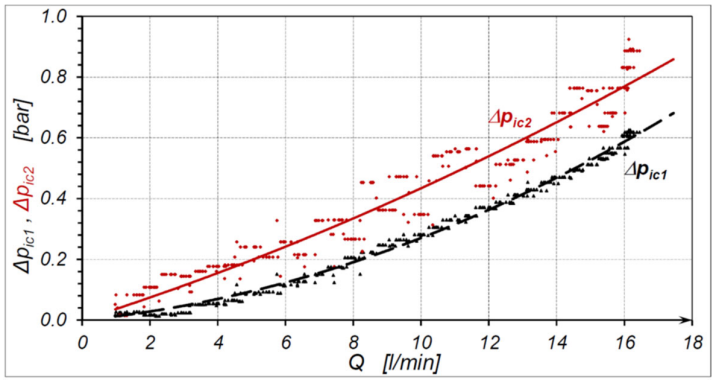

Figure 17. Characteristics of the pressure drop $\Delta p_{ic1} = f(Q)$ and $\Delta p_{ic2} = f(Q)$ in internal channel of the motor (no cavitation)—motor supplied with oil [23].

7.4. Compression of Liquid in Working Chamber

Experimental data (Figure 12 and Figure 17) show that, in a motor with zero overlap in the commutation units, for one direction of the flow rate (from port *A* to port *B*), $\Delta p_{ic1} \neq \Delta p_{ic2}$. Therefore, there is a pressure increase Δp_{HPC} caused by the compression of liquid in a closed working chamber. Characteristics of $\Delta p_{HPC} = f(n)$ in the motor supplied with water and supplied with oil are shown in Figure 18. These characteristics are proposed to describe by the empirical formula in the form:

- For water:

$$\Delta p_{HPC} = 0.635 \cdot 10^{-4} \cdot \mathrm{n}^{1.3} \quad (16)$$

- For oil:

$$\Delta p_{HPC} = 1.1 \cdot 10^{-4} \cdot \mathrm{n}^{1.14} \quad (17)$$

Therefore, the assumption described by Formula (7) is not true.

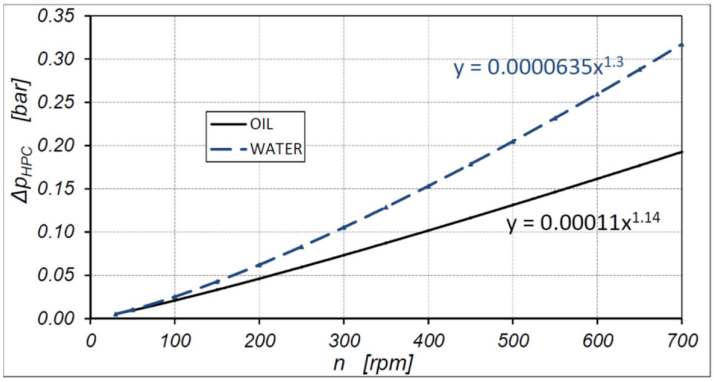

Figure 18. Characteristics of the pressure increase $\Delta p_{HPC} = f(n)$ calculated according to Formula (9)—motor supplied with oil and water.

7.5. Pressure Drop in Internal Channel

Characteristic of $\Delta p_{ich} = f(Q)$ in the motor supplied with water is shown in Figure 19, and in the motor supplied with oil is shown in Figure 20.

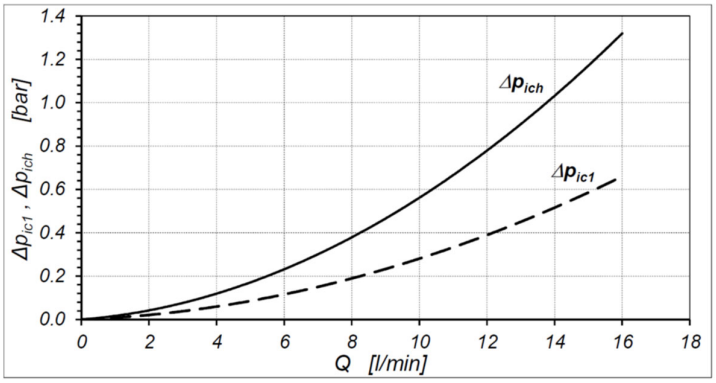

Figure 19. Characteristics of the total pressure drop $\Delta p_{ich} = f(Q)$ in the motor and the pressure drop $\Delta p_{ic1} = f(Q)$ in one internal channel of the motor—motor supplied with water [23].

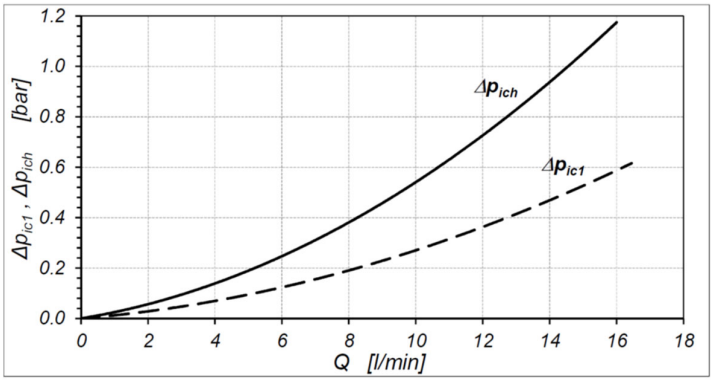

Figure 20. Characteristics of the total pressure drop $\Delta p_{ich} = f(Q)$ in the motor and the pressure drop $\Delta p_{ic1} = f(Q)$ in one internal channel of the motor—motor supplied with oil [23].

Characteristics of $\Delta p_{ic1} = f(Q)$, shown in Figures 19 and 20, can be described by Equation (13). The value of constants C_t and C_l are:

(a) For water: $C_t = 7.88 \times 10^8$ and $C_l = 409.8 \times 10^8$;
(b) For oil: $C_t = 6.73 \times 10^8$ and $C_l = 19.2 \times 10^8$.

Whereas the total pressure drop in the motor, according to Formulas (13) and (3), is:

(a) For water:

$$\Delta p_{ich} = 1576 \cdot \rho \cdot Q^2 + 81960 \cdot \nu \cdot \rho \cdot Q \text{ MPa} \quad (18)$$

(b) For oil:

$$\Delta p_{ich} = 1346 \cdot \rho \cdot Q^2 + 3840 \cdot \nu \cdot \rho \cdot Q \text{ MPa} \quad (19)$$

The ratio $\Delta p_{ich,W}/\Delta p_{ich,O}$ is shown in Figure 21 ($\Delta p_{ich,W}$ and $\Delta p_{ich,O}$—pressure drop in the internal channels of the motor supplied with water an oil, respectively).

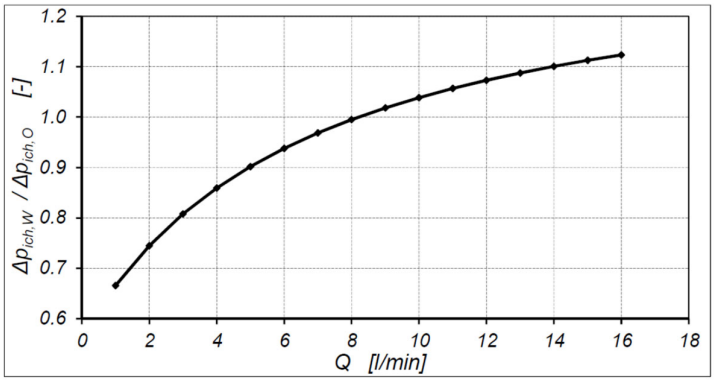

Figure 21. Characteristics of the ratio of pressure drops $\Delta p_{ich,W}/\Delta p_{ich,O} = f(Q)$—result of experiment.

In the range of a low flow rate Q (up to 8 L/min) a smaller pressure drop Δp_{ich} in the motor supplied with water was observed. However, in the range of a high flow rate, a smaller pressure drop was in the motor supplied with oil. This difference can be explained as follows. At a low flow rate, the share of the laminar flow component is larger than at a high flow rate. Because the viscosity of water is about 40 times lower than the viscosity of oil, a lower pressure drop in the motor supplied with water is at a low flow rate. However, at a high flow rate, the share of the laminar flow component is very small and the turbulent component is dominant. The biggest influence on the pressure drop during turbulent flow is the density of the liquid. Therefore, at a high flow rate, the pressure drop in the internal channels is smaller in the motor supplied with oil [29].

8. CFD Calculations

8.1. Method of Calculations

Numerical calculations of the liquid flow in the motor were carried out using the ANSYS Workbench program. The calculation module CFX and calculation model SST (Shear Stress Transport) were used. Some researchers, such as [33–38], applied the k-ε model to the calculation of the flow in hydraulic elements. However, the SST model contains features of the k-ε model and the k-ω model. Furthermore, the SST model ensures a faster convergence of results. For issues such as calculating the flow in the internal channels of a hydraulic motor, the SST model is sufficient.

8.2. The Geometry of Liquid in the Motor and Simplifying the Calculation Model

The geometry of liquid in a hydraulic motor is the geometry of the internal channels in the motor and the geometry of the working chambers. The following simplifications concerning models of the geometry of liquid in a satellite motor are used:

(a) The commutation plate (6) (Figure 9 and Figure 11) is rotated relative to plate (7) by 30°. In this way, the *OC* holes (Figure 11) in the commutation plate (6) are opposite the *OC* holes in the commutation plate (7). Then, there is a free flow of liquid through the working mechanism and this mechanism does not rotate (is stationary);

(b) All of the calculations were carried out for one casual position of the working mechanism;
(c) Six working chambers were omitted—in these chambers the flow of liquid does not occur. Only four *OC* holes in the commutation plate allowed liquid flow by the working chambers (Figure 10);
(d) A leak in the gaps of the working mechanism was omitted;
(e) Tooth profiles in satellites, the curvature and the rotor were omitted. The satellites have been replaced by cylinders with diameters equal to the pith diameter of the satellite. In the rotor and curvature, the tooth profiles were replaced by a smooth profile according to the pitch line of tooth (Figure 22);

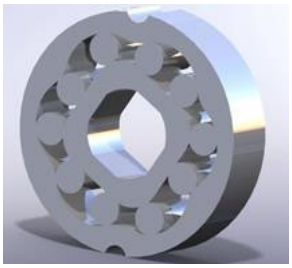

Figure 22. Simplified satellite working mechanism [28].

(f) An outline of the threads was omitted and replaced by cylinders with diameters equal to pith diameters of threads;
(g) Necks in the body and in the collectors were removed—there is no liquid flow in these elements and these elements have no significant influence on the pressure drop;
(h) The roughness of the walls was omitted.

The simplified calculation model of the satellite motor is shown in Figure 23.

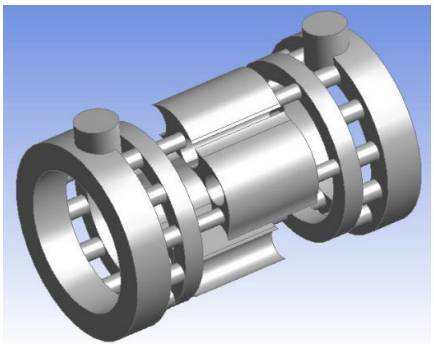

Figure 23. Simplified model of liquid volume in the motor [28].

8.3. The Mesh

In order to obtain reliable results from the simulation, it is necessary to create the best elements mesh. The uneven division into finite elements is a common issue. In areas where the wanted function changes rapidly, there is a denser mesh of elements. In contrast, in areas where the function changes slowly, there is a less dense mesh. The size of the mesh elements was selected by comparing the results of calculations with different sizes of finite elements. Finally, a mesh was chosen that gave an error of less than 5% in relation to the denser mesh.

The following discretization parameters were used to create the mesh:

- General size of finite elements is 0.6 mm;
- On the edges (like at changes in the diameter of the channel) more dense mesh is applied (the size of a single element is 0.25 mm).

Furthermore, a boundary layer was defined on all channel walls. The thickness of this layer depends on the dimensions of the channel. For channels with a smaller diameter, a layer with a smaller thickness was assigned. Therefore, in *OC* holes in the commutation plates (Figure 11) and in holes in low- and high-pressure manifolds (3) and (4) (Figure 9), ten boundary layers with a thickness of 0.2 mm were defined (increment coefficient 1.2). In the other channels, 18 boundary layers with a thickness of 0.3 mm were defined (increment coefficient also 1.2).

In this way, the mesh of elements was obtained (Figure 24). This mesh consisted of 3,992,282 finite elements and 1,367,996 nodes.

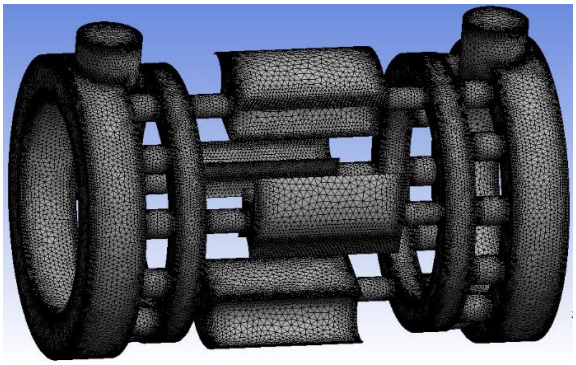

Figure 24. The mesh of elements of liquid in the internal channels of the motor [28].

8.4. Boundary Conditions

The boundary conditions are as follows:

- Defining the inflow (Figure 25a)—the wall that simulates inflow of the working liquid. As a kind of boundary condition, "Mass Inlet" was selected;
- Defining the outflow (Figure 25b)—the wall that simulates outflow of the working liquid. The value of the pressure on the outflow wall was assumed to be 0 bar (p = 0 bar);
- Defining the walls in contact with the liquid (Figure 25c)—the other walls of the model that define the shape and boundaries of the liquid. They were assigned a boundary condition in the form of "wall" with a slip limitation.

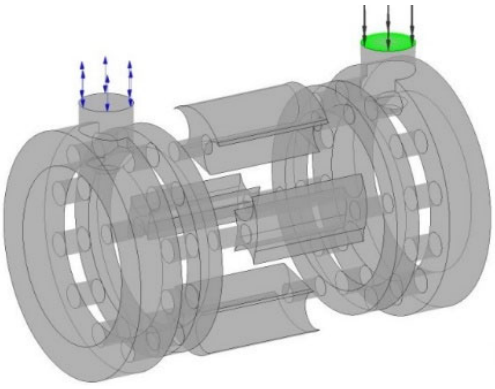

(**a**)

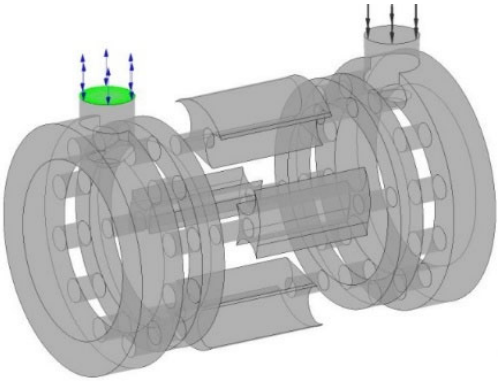

(**b**)

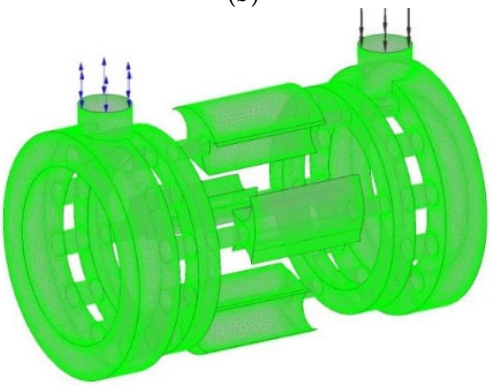

(**c**)

Figure 25. Defined boundary conditions in a model of the liquid [28]: (**a**) inflow, (**b**) outflow, (**c**) wall.

In order to determine the characteristics of the pressure drop in the internal channels of the motor, the calculations were carried out in several steps for different values of the flow rate (Table 1). All calculations were conducted in one calculation series.

Table 1. Calculation steps and the corresponding flow rate.

No. of Step	1	2	3	4	5	6	7	8	9	10
[L/min]	2.0	4.0	6.0	8.0	10.0	12.0	14.0	16.0	18.0	20.0
[kg/s]	0.033	0.066	0.100	0.133	0.166	0.200	0.233	0.266	0.300	0.333

8.5. Parameters of the Liquids

Defining the parameters of water is limited to loading these parameters from the database offered by Ansys and determining the water temperature. Therefore, for water:

- The density $\rho = 999.8$ kg/m^3;
- The kinematic viscosity $\nu = 0.89$ cSt;
- The temperature $T = 25$ °C.

Ansys does not have oil parameters in its database. Therefore, it is necessary to define the parameters for oil. In the calculations, it was assumed:

- The density $\rho = 862$ kg/m^3;
- The kinematic viscosity $\nu = 40$ cSt;
- The temperature $T = 43$ °C.

It was assumed that water and oil are incompressible and their properties are constant.

8.6. The Conditions of the Simulations

The target value for the convergence of results has been defined—the residual value was set to 0.0001.

It was assumed that the simulation is stationery.

Before starting the calculations, it was necessary to define the number of processors that were used to perform computer calculations. In the described case, eight processors were used.

8.7. Results of the Calculations

In a later part of this article, an example of the velocity distribution and the pressure drop in the internal channels of the motor for a water and oil flow rate equal to 10 L/min are presented.

The distribution of water and oil velocity in the internal channels of the motor are shown in Figures 26–28, but the pressure distribution is shown in Figures 29 and 30. respectively.

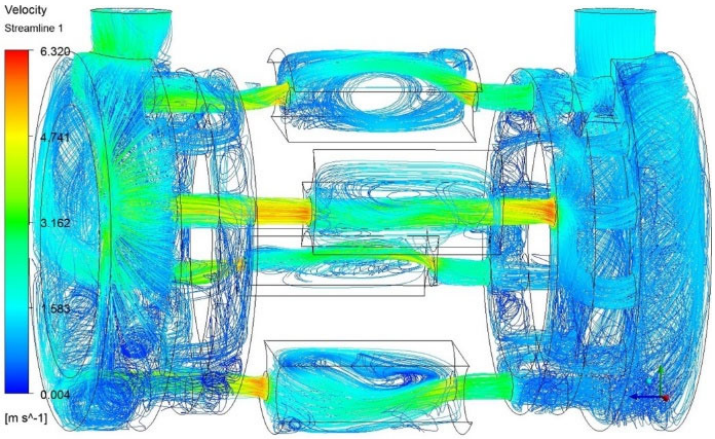

Figure 26. Distribution of water velocity in the internal channels of the motor (flow rate Q = 10 L/min) [28].

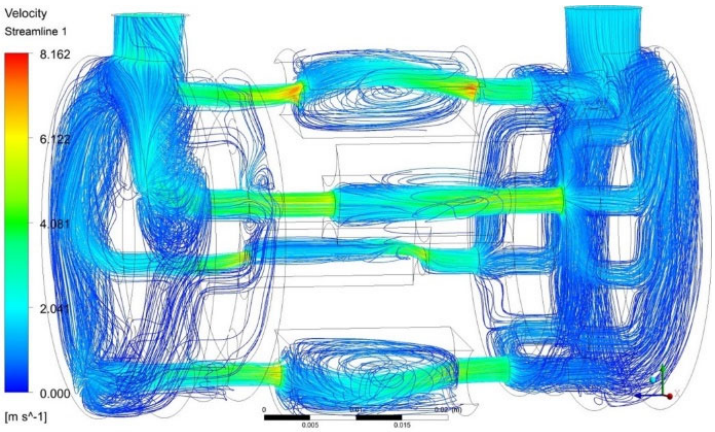

Figure 27. Distribution of oil velocity in the internal channels of the motor (flow rate Q = 10 L/min) [28].

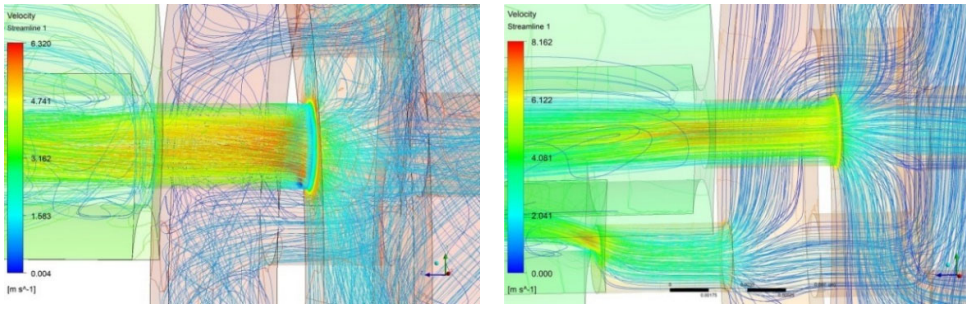

Figure 28. Distribution of water velocity (**left figure**) and oil velocity (**right figure**) in hole *OC* in commutation plate [28].

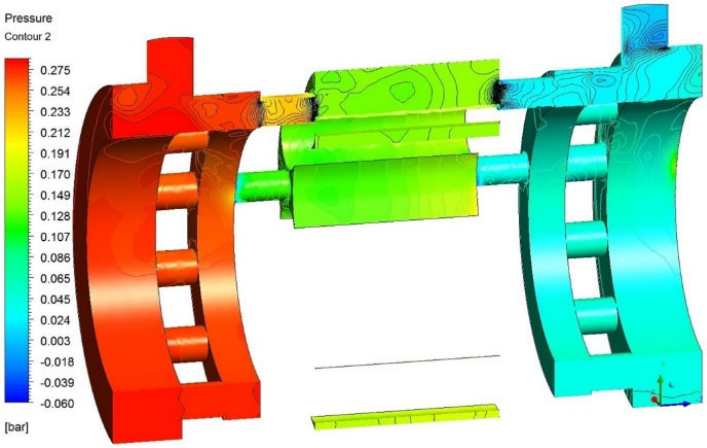

Figure 29. Distribution of water pressure in the internal channels of the motor (flow rate Q = 10 L/min) [28].

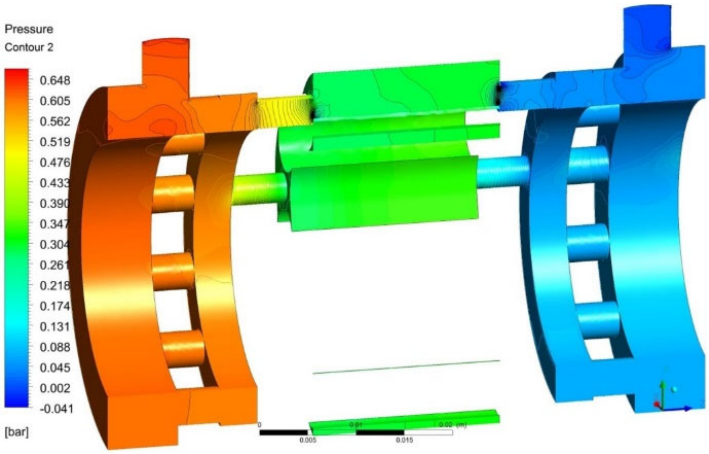

Figure 30. Distribution of oil pressure in the internal channels of the motor (flow rate Q = 10 L/min) [28].

The liquid flow area is the smallest in the holes of the commutation unit plates. Therefore, the highest pressure drop and the highest liquid flow velocities can be found in these holes (Figures 31 and 32).

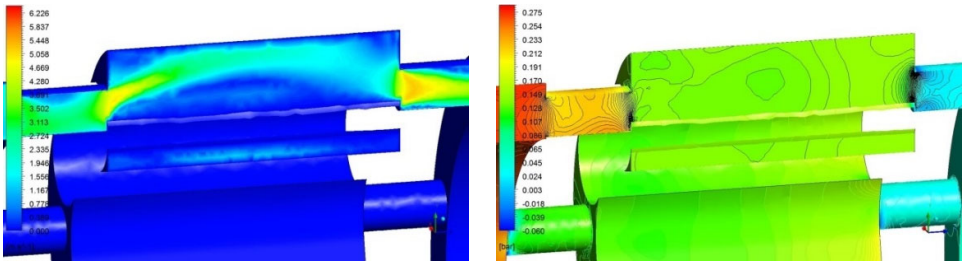

Figure 31. Distribution of water velocity (**left figure**) and distribution of water pressure (**right figure**) in the commutation holes *OC* and in the working chamber of the motor (flow rate $Q = 10$ L/min). The holes *OC* in the commutation plates are partially obscured by the satellite [28].

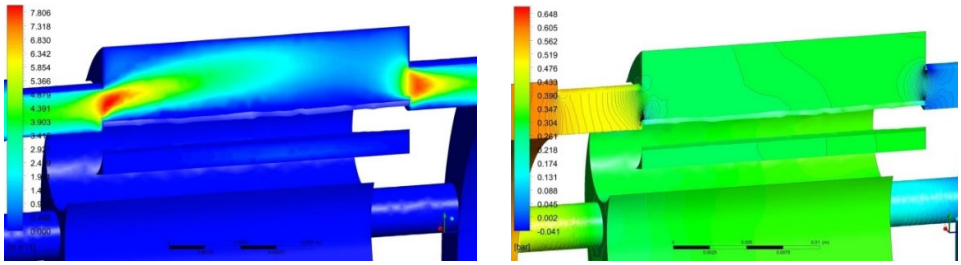

Figure 32. Distribution of oil velocity (**left figure**) and distribution of oil pressure (**right figure**) in the commutation holes *OC* and in the working chamber of the motor (flow rate $Q = 10$ L/min). The holes *OC* in the commutation plates are partially obscured by the satellite [28].

In order to determine the characteristics of the pressure drop as a function of the flow path in the internal channels of the motor, a line was defined as in Figure 33 (by the inflow and outflow ports, the inflow and outflow manifolds, the holes in the commutation unit plate and the working chamber). It should be noted that the holes in the commutation unit plate are completely open.

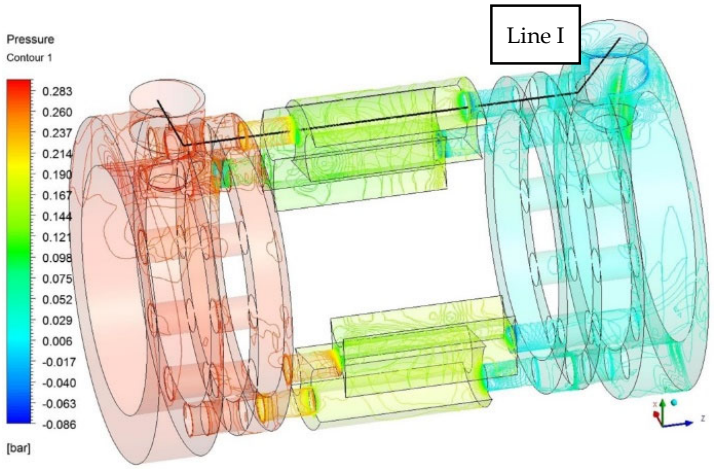

Figure 33. The course of "Line I" helping to determine the characteristic of the pressure drop in the internal channels of the motor [28].

Characteristics of the average liquid flow velocity and the average pressure in the internal channel of the motor are shown in Figures 34 and 35. These characteristics show that the largest pressure differences were between the hole of the commutation unit plate and the working chamber.

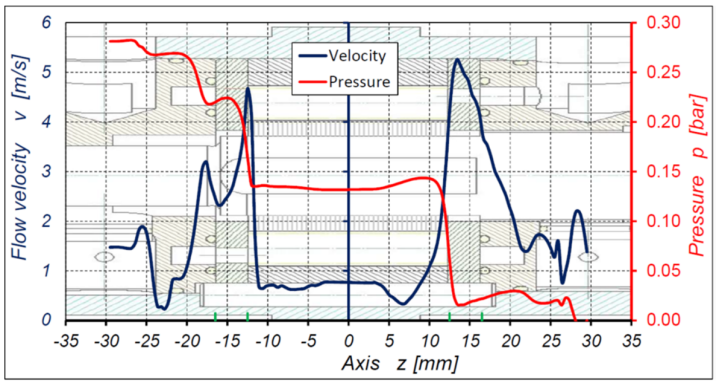

Figure 34. Characteristics of the average water flow velocity v and water pressure p in the internal channels of the motor as a function of the path "z" (the "z" path coincides with the axis of the motor shaft). Results of CFD calculation for the flow rate Q = 10 L/min. The *OC* holes in the commutation unit plates are completely open.

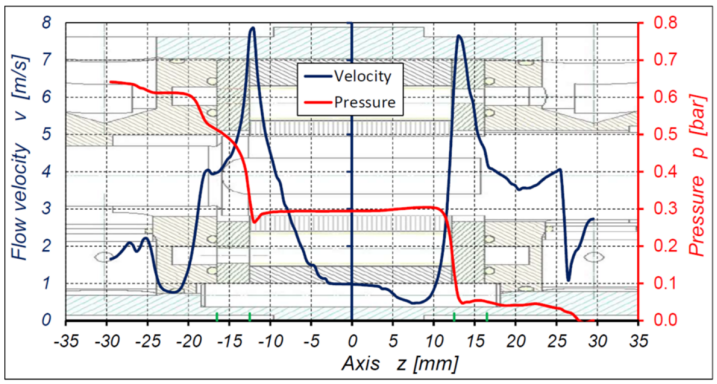

Figure 35. Characteristics of the average oil flow velocity v and oil pressure p in the internal channels of the motor as a function of the path "z" (the "z" path coincides with the axis of the motor shaft). Results of CFD calculation for the flow rate Q = 10 L/min. The *OC* holes in the commutation unit plates are completely open.

8.8. Pressure Drop in the Internal Channel of the Motor

It was assumed that the *OC* holes in commutation plate 6 (according to Figure 9) are opposite the *OC* holes in commutation plate 7. This caused some of the holes in commutation plates to be obscured by the satellite (each hole to a different degree). Thus, the fluid flow fields in holes of the commutation plates were different. As a result, the flow velocities and pressure drop in these holes were also different. Therefore, the pressure in the working chambers were also different. Thus, the statement that the pressure drop in the internal channel should be understood as the pressure difference in the motor ports and in any given working chamber gives an incorrect result. For confirmation, the pressure drop $\Delta p_{ic1\text{-}!!}$ in internal low-pressure channels, the pressure drop $\Delta p_{ic2\text{-}!!}$ in internal high-pressure channels and the total pressure drop $\Delta p_{ich\text{-}!!}$ along line 1 (from Figure 33) were calculated (Figures 36 and 37).

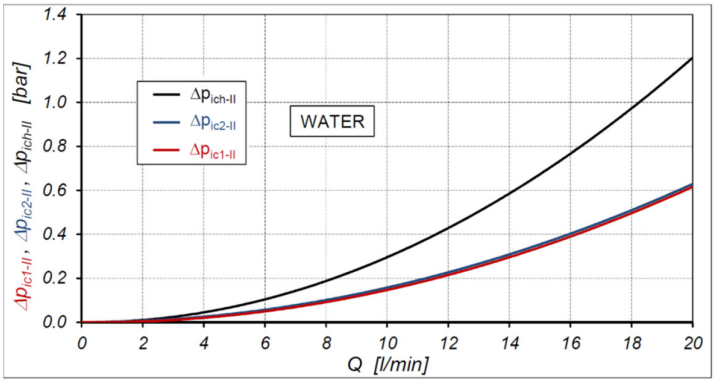

Figure 36. Characteristics of the pressure drop $\Delta p_{ic1-!!} = f(Q)$. $\Delta p_{ic2-!!} = f(Q)$ and $\Delta p_{ich-!!} = f(Q)$ in the internal channels of the motor supplied with water—results of CFD calculations.

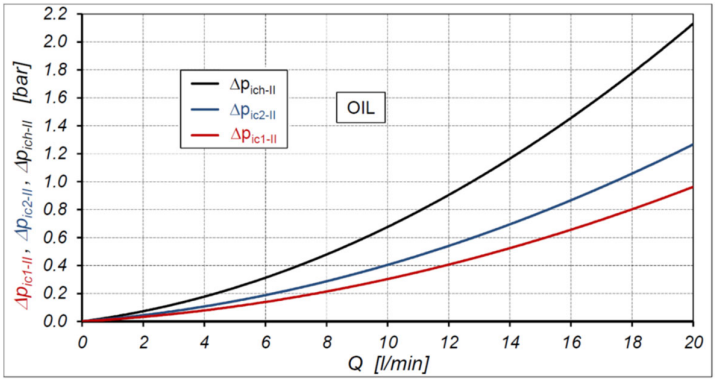

Figure 37. Characteristics of the pressure drop $\Delta p_{ic1-!!} = f(Q)$, $\Delta p_{ic2-!!} = f(Q)$ and $\Delta p_{ich-!!} = f(Q)$ in the internal channels of the motor supplied with oil—results of CFD calculations.

The ratio of the pressure drops $\Delta p_{ich,W}/\Delta p_{ich,O}$ in the internal channels of the motor supplied with water and supplied with oil is shown in Figure 38.

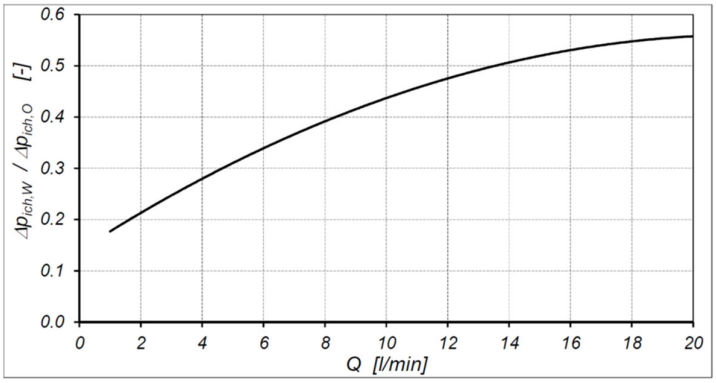

Figure 38. Characteristic of $\Delta p_{ich,W}/\Delta p_{ich,O} = f(Q)$. $\Delta p_{ich,W}$ and $\Delta p_{ich,O}$—pressure drop in the internal channels of the motor supplied with water and supplied with oil. Result of simulation.

In contrast to the results of experiment, the results of the CFD calculations showed that in all ranges of flow rate the pressure drop in the internal channels of the motor supplied with water is smaller than that supplied with oil. This is a significant difference in results of simulation compared to the results of the experiment. Most likely, this difference is the result of the adopted simplifications in the model—mainly by stopping the satellite mechanism and setting the holes in commutation plates opposite each other.

9. Conclusions

The results of the experimental research showed that:

(a) The type of liquid and the parameters of the liquid (kinematic viscosity and density) have a big influence on the pressure drop in the internal channels of the hydraulic motor;
(b) The flow in the internal channels of the motor is not a fully developed turbulent flow. This applies to both water and mineral oil;
(c) Low flow rate in the motor (up to 8 L/min) for water is a lower pressure drop than for oil, but regarding high flow rate oil is a lower pressure drop;
(d) The value of the pressure p_{LPC} in the suction chamber (low-pressure chamber *(LPC))* (Figure 10) of the satellite motor depends on the type of liquid (in the motor supplied with oil the pressure p_{LPC} is −0.75 bar, but in the motor supplied with water the p_{LPC} is −0.85 bar);
(e) It is possible to test the pressure drop in internal channels of a hydraulic motor according to the proposed method without measuring the pressure in the working chambers. Then, the presented above values of pressure p_{LPC} should be taken instead of value p_{LPC} = −1 bar;
(f) The pressure drop in both the internal low-pressure channels (inflow channels) and in the internal high-pressure channels (outflow channels) in the hydraulic motor can be described with Formula (13);
(g) If the volume of the working chamber tends to the minimum, then in this chamber additional increase of pressure Δp_{HPC} occurs. This pressure depends on the overlap in the commutation unit and also depends on the rotational speed of the motor. Therefore, the Δp_{HPC} is not the component of pressure losses in the internal channels of the motor. The Δp_{HPC} has influence only on mechanical losses in the working mechanism of the motor.

The results of the CFD calculation have shown that it is possible to carry out the numerical calculation of flow in the internal channel of the motor but only with substantial assumptions and simplifications. This simplification does not fully reflect the phenomena occurring in the motor.

The CFD calculation showed that the biggest pressure drop is in the holes of the commutation unit plates, regardless of the type of liquid.

The values of the pressure drop in the internal channels of the motor obtained from the experiment (Figures 19 and 20) differ from the results obtained by CFD calculations (Figures 36 and 37). The differences are shown in Figure 39.

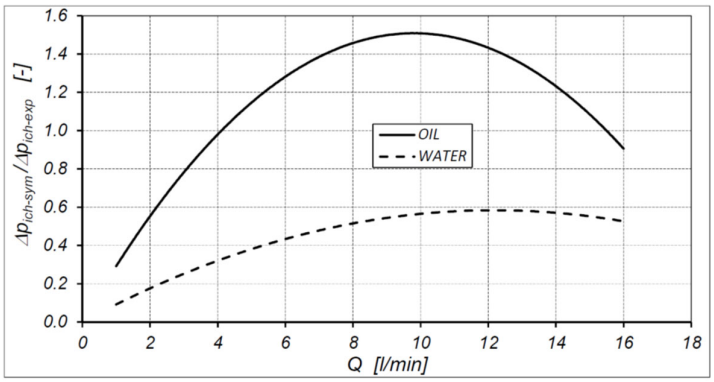

Figure 39. Characteristics of $\Delta p_{ich\text{-}sym}/\Delta p_{ich\text{-}exp} = f(Q)$. $\Delta p_{ich\text{-}sym}$—pressure drop in the internal channels calculated numerically (CFD); $\Delta p_{ich\text{-}exp}$—pressure drop in the internal channels obtained experimentally. Motor supplied with water and with oil.

The main reasons for the differences are:

(a) The simplifying of the calculation model by stopping the satellite mechanism and setting the holes in commutation plates opposite each other;
(b) The impossibility of simulating the pressure difference in the working chambers for a rotating satellite mechanism;
(c) Difficultly of researching dynamic phenomena that occur in the working chambers during the operation of the satellite mechanism.

As the final conclusions, it should be stated that:

(a) The CFD calculation can only estimate the pressure drop in the internal channels of the motor. The underestimation can be up to 50%;
(b) The CFD method has some advantages over the experimental method. Namely, it allows the velocity and pressure distribution in the internal channels with an irregular, complicated shape to be determined.

In the future, it should be attempted to simulate flow in a satellite motor without major simplification, i.e., with a working (rotating) satellite mechanism.

Author Contributions: Conceptualization, P.S.; methodology, P.S.; software, P.P.; validation, P.P. and P.S.; formal analysis, P.S.; investigation, P.S.; resources, P.S. and P.S.; data curation, P.S.; writing—original draft preparation, P.S.; writing—review and editing, P.S.; visualization, P.P.; supervision, P.S.; project administration, P.S.; funding acquisition, P.S. All authors have read and agreed to the published version of the manuscript.

Funding: This research was funded by the National Centre for Research and Development in Poland, grant number LIDER/35/102/L-2/10/NCBiR/2011.

Conflicts of Interest: The authors declare no conflict of interest.

References

1. Guzowski, A.; Sobczyk, A. Reconstruction of hydrostatic drive and control system dedicated for small mobile platform. In *Fluid Power Systems Technology*; American Society of Mechanical Engineers: New York, NY, USA, 2014; doi:10.1115/FPNI2014-7862.
2. Pobedza, J.; Sobczyk, A. Properties of high-pressure water hydraulic components with modern coatings. In *Advanced Materials Research*; Trans Tech Publications Ltd.: Stafa-Zurich, Switzerland, 2014; Volume 849, doi:10.4028/www.scientific.net/AMR.849.100.
3. Litwin, W.; Olszewski, A. Water-lubricated sintered bronze journal bearings—Theoretical and experimental research. *Tribol. Trans.* **2014**, *57*, 114–122, doi:10.1080/10402004.2013.856980.
4. Walczak, P.; Sobczyk, A. Simulation of water hydraulic control system of Francis turbine. In *Fluid Power Systems Technology*; American Society of Mechanical Engineers: New York, NY, USA, 2014, doi:10.1115/FPNI2014-7814.
5. Dymarski, C.; Dymarski, P. Developing methodology for model tests of floating platforms in low-depth towing tank. *Arch. Civ. Mech. Eng.* **2016**, *16*, 159–167, doi:10.1016/j.acme.2015.07.003.
6. Lubinski, J.; Sliwinski, P. Multi parameter sliding test result evaluation for the selection of material pair for wear resistant components of a hydraulic motor dedicated for use with environmentally friendly working fluids. In *Solid State Phenomena*; Trans Tech Publications Ltd.: Stafa-Zurich, Switzerland, 2015; Volume 225, doi:10.4028/www.scientific.net/SSP.225.115.
7. Urbanczyk, J. Research of Hydraulic Motors for Needs of Small Mechanization in the Mining Industry. Ph.D. Thesis, AGH University of Science and Technology, Cracow, Poland, 1999.
8. Sliwinski, P. The methodology of design of axial clearances compensation unit in hydraulic satellite displacement machine and their experimental verification. *Arch. Civ. Mech. Eng.* **2019**, *19*, 1163–1182, doi:10.1016/j.acme.2019.04.003.
9. Maczyszyn, A. Energy Analysis of Rotary Positive Displacement Machines Used in Hydrostatic Transmissions. Ph.D. Thesis, Gdansk University of Technology, Gdansk, Poland, 2014.
10. Osinski, P.; Deptula, A.; Partyka, M. Discrete optimization of a gear pump after tooth root undercutting by means of multivalued logic trees. *Arch. Civ. Mech. Eng.* **2013**, *13*, 422–431, doi:10.1016/j.acme.2013.05.001.
11. Stosiak, M.; Zawislak, M.; Nishta, B. Studies of resistances of natural liquid flow in helical and curved pipes. *Pol. Marit. Res.* **2018**, *3*, 123–130, doi:10.2478/pomr-2018-0103.
12. Osinski, P.; Warzynska, U.; Kollek, W. The influence of gear micropump body asymmetry on stress distribution. *Pol. Marit. Res.* **2017**, *24*, 60–65, doi:10.1515/pomr-2017-0007.
13. Jasinski, R. Problems of the starting and operating of hydraulic components and systems in low ambient temperature (Part III). *Pol. Marit. Res.*, **2009**, *4*, 22–31, doi:10.2478/v10012-008-0052-2.
14. Jasinski, R. Problems of the starting and operating of hydraulic components and systems in low ambient temperature (Part IV). *Pol. Marit. Res.* **2017**, *3*, 45–57, doi:10.1515/pomr-2017-0089.
15. Paszota, Z. *Energy Losses in Hydrostatic Drive*; LABERT Academic Publishing: Saarbrücken, Germany, 2016.

16. Saheban Alahadi, M.J.; Shirneshan, A.; Kolahdoozan, M. Experimental investigation of the effect of grooves cut over the piston surface on the volumetric efficiency of a radial hydraulic piston pump. *Int. J. Fluid Power* **2017**, *18*, 181–187, doi:10.1080/14399776.2017.1337440.
17. Balawender, A. Energy analysis and methodics of testing of low-speed hydraulic motors. In *Scientific Book of the Gdansk University of Technology*; Mechanika, No. 54; Gdansk University of Technology Publishing House: Gdansk, Poland, 1988.
18. Zaluski, P. Influence of the Position of the Swash Plate Rotation Axis on the Volumetric Efficiency of Axial Piston Pumps. Ph.D. Thesis, Gdansk University of Technology, Gdansk, Poland, 2017.
19. Zaluski, P. *Experimental Research of an Axial Piston Pump with Displaced Swash Plate Axis of Rotation*; Lecture Notes in Mechanical Engineereing. Advances in Hydraulic and Pneumatic Drives and Control 2020; Springer Nature Switzerland AG: Cham, Switzerland, 2021; doi:10.1007/978-3-030-59509-8_12.
20. Sliwinski, P. The influence of water and mineral oil on volumetric losses in hydraulic motor. *Pol. Marit. Res.* **2017**, *S1*, 213–223, doi:10.1515/pomr-2017-0041.
21. Sliwinski, P. The flow of liquid in flat gaps of satellite motors working mechanism. *Pol. Marit. Res.* **2014**, *2*, 125–135, doi:10.2478/pomr-2014-0019.
22. Sliwinski, P. The influence of water and mineral oil on the leaks satellite motor commutation unit clearances. *Pol. Marit. Res.* **2017**, *3*, 58–67, doi:10.1515/pomr-2017-0090.
23. Sliwinski, P. *Satellite Displacement Machines. Basic of Design and Analysis of Power Loss*; Gdansk University of Technology Publishers: Gdansk, Poland, 2016.
24. Patrosz, P. Influence of properties of hydraulic fluid on pressure peaks in axial piston pumps' chambers. *Energies* **2021**, *14*, 3764, doi:10.3390/en14133764.
25. Patrosz, P. *Influence of Gaps' Geometry Change on Leakage Flow in Axial Piston Pumps*; Lecture Notes in Mechanical Engineereing. Advances in Hydraulic and Pneumatic Drives and Control 2020; Springer Nature Switzerland AG: Cham, Switzerland, 2021; doi:10.1007/978-3-030-59509-8_7.
26. Skorek, G. Laboratory tests of pressure losses in a displacement pump. *Hydraulika i Pneumatyka* **2005**, *2*, 12–15.
27. Balawender, A. Physical and mathematical model of losses in hydraulic motors. In *Developments in Mechanical Engineering*; Gdansk University of Technology Publishers, Gdansk, Poland, 2005.
28. Maciejewski, M. Komputerowe Obliczenia Spadków Ciśnienia w Kanałach Wewnętrznych Silnika Satelitowego. Master's Thesis, Faculty of Mechanical Engineering, Gdansk University of Technology, Gdansk, Poland, 2013.
29. Sliwinski, P.; Patrosz, P. The influence of water and mineral oil on pressure losses in hydraulic motor. In *Lecture Notes in Mechanical Engineering*; Cavas-Martínez, F., Chaari, F., Gherardini, F., Haddar, M., Ivanov, V., Kwon, Y.W., Trojanowska, J., di Mare, F., Eds.; Springer International Publishing: Geneva, Switzerland, 2020; doi:10.1007/978-3-030-59509-8_10.
30. Sliwinski, P. Determination of the theoretical and actual working volume of a hydraulic motor. *Energies* **2020**, *13*, 5933, doi:10.3390/en13225933.
31. Sliwinski, P. Determination of the theoretical and actual working volume of a hydraulic motor—Part II (The method based on the characteristics of effective absorbency of the motor). *Energies* **2021**, *14*, 1648, doi:10.3390/en14061648.
32. Sliwinski, P. Pressure Losses and Power Balance in the Unloaded Satellite Pump. *Hydraulika Pneumatika* **2013**, *5*, 39–45.
33. Amirante, R.; Moscatelli, P.; Catalano, L. Evaluation of the flow forces on a direct (single stage) proportional valve by means of a computational fluid dynamic analysis. *Energy Convers. Manag.* **2007**, *48*, 942–953, doi:10.1016/j.enconman.2006.08.024.
34. Chattopadhyay, H.; Kundu, A.; Saha, B.; Gangopadhyay, T. Analysis of flow structure inside a spool type pressure regulating valve. *Energy Convers. Manag.* **2012**, *53*, 196–204, doi:10.1016/j.enconman.2011.08.021.
35. Domagala, M. CFD analysis of a flow control valve. In proceedings of the 5th FPNI PhD Symposium, Cracow, Poland, 1–5 July 2008.
36. Lisowski, E.; Czyzycki, W.; Rajda, J. Three dimensional CFD analysis and experimental test of flow force acting on the spool of solenoid operated directional control valve. *Energy Convers. Manag.* **2013**, *70*, 220–229, doi:10.1016/j.enconman.2013.02.016.
37. Lisowski, E.; Filo, G.; Rajda, J. Pressure compensation using flow forces in a multi-section proportional directional control valve. *Energy Convers. Manag.* **2015**, *103*, 1052–1064, doi:10.1016/j.enconman.2015.07.038.
38. Lisowski, E.; Rajda, J. CFD analysis of pressure loss during flow by hydraulic directional control valve constructed from logic valves. *Energy Convers. Manag.* **2013**, *65*, 285–291, doi:10.1016/j.enconman.2012.08.015.